Polarized PtdIns(4,5)P_2 distribution mediated by a voltage-sensing phosphatase (VSP) regulates sperm motility

Takafumi Kawai[a], Haruhiko Miyata[b], Hiroki Nakanishi[c], Souhei Sakata[a,1], Shin Morioka[d,e], Junko Sasaki[d,f], Masahiko Watanabe[g], Kenji Sakimura[h], Toyoshi Fujimoto[i,2], Takehiko Sasaki[d,f], Masahito Ikawa[b], and Yasushi Okamura[a,j,3]

[a]Graduate School of Medicine, Osaka University, Suita 565-0871, Japan; [b]Research Institute for Microbial Diseases, Osaka University, Suita 565-0871, Japan; [c]Research Center for Biosignal, Akita University, Akita 010-8543, Japan; [d]Medical Research Institute, Tokyo Medical and Dental University, Tokyo 113-8510, Japan; [e]Graduate School of Biomedical and Health Sciences, Hiroshima University, Hiroshima 734-8553, Japan; [f]Graduate School of Medicine, Akita University, Akita 010-8543, Japan; [g]Graduate School of Medicine, Hokkaido University, Sapporo 060-8638, Japan; [h]Brain Research Institute, Niigata University, Niigata 951-8585, Japan; [i]Graduate School of Medicine, Nagoya University, Nagoya 466-8550, Japan; and [j]Graduate School of Frontier Bioscience, Osaka University, Suita 565-0871, Japan

Edited by David E. Clapham, Howard Hughes Medical Institute, Janelia Research Campus, Ashburn, VA, and approved October 31, 2019 (received for review September 28, 2019)

The voltage-sensing phosphatase (VSP) is a unique protein that shows voltage-dependent phosphoinositide phosphatase activity. Here we report that VSP is activated in mice sperm flagellum and generates a unique subcellular distribution pattern of PtdIns(4,5)P_2. Sperm from VSP$^{-/-}$ mice show more Ca^{2+} influx upon capacitation than VSP$^{+/-}$ mice and abnormal circular motion. VSP-deficient sperm showed enhanced activity of Slo3, a PtdIns(4,5)P_2-sensitive K^+ channel, which selectively localizes to the principal piece of the flagellum and indirectly enhances Ca^{2+} influx. Most interestingly, freeze-fracture electron microscopy analysis indicates that normal sperm have much less PtdIns(4,5)P_2 in the principal piece than in the midpiece of the flagellum, and this polarized PtdIns(4,5)P_2 distribution disappeared in VSP-deficient sperm. Thus, VSP appears to optimize PtdIns(4,5)P_2 distribution of the principal piece. These results imply that flagellar PtdIns(4,5)P_2 distribution plays important roles in ion channel regulation as well as sperm motility.

voltage-sensing phosphatase | membrane potential | PtdIns(4,5)P_2 | sperm

It is widely known that phosphoinositides (PIPs) play pivotal roles in controlling a variety of cellular physiological processes (1), including the regulation of physiological properties of diverse ion channels and transporters (2, 3). Over a decade ago, we reported a voltage-sensing phosphatase (VSP) that contains a voltage-sensor domain, as found in conventional voltage-gated ion channels, but contains a PTEN-like phosphatase domain instead of a pore-gate domain (4). The VSP shows voltage-dependent phosphatase activity toward PIPs (4), and thus directly converts electrical signals into chemical signals (3). While these unique molecular properties were first discovered for a sea squirt (*Ciona intestinalis*) VSP (Ci-VSP), by expression in *Xenopus* oocytes (4), VSPs are also widely conserved in vertebrates (3). Biophysical mechanisms underlying the voltage-dependent phosphatase activity have been intensively investigated (3), but the physiological roles of VSPs still remain unclear in any animal species.

The previous studies suggested that the VSP is commonly expressed in testis (3). We previously demonstrated that VSP protein is present on the plasma membrane of the sperm flagellum in *C. intestinalis*, by immunoelectron microscopy (4). These lines of evidence raise the possibility that the VSP may have a physiologically important function in sperm and fertilization.

Recent electrophysiological experiments demonstrated that mouse sperm contain several types of ion channels and transporters that are essential for fertilization; CatSper (Ca^{2+} channel) (5, 6), Slo3 (K^+ channel) (7, 8), sNHE (Na^+-H^+ exchanger) (9), and PMCA4 (Ca^{2+} pump) (10). These transmembrane proteins are responsible for dynamic changes in physiological status of sperm, and absence of these genes results in male infertility (5–10). Therefore, any modulation of each of these ion channels and transporters by PIPs should importantly influence the physiological function of sperm.

In the present study, to investigate the physiological function of VSP in mouse sperm, we analyzed a VSP-deficient mouse line. We report that VSP provides a mode of regulation of ion channel activity by PIPs.

Results

VSP-Deficient Sperm Show Abnormal Motility during Capacitation. We confirmed that mRNA encoding the VSP is expressed in spermatocytes in mouse testis using in situ hybridization (*SI Appendix*, Fig. S1*A*). Furthermore, we also detected the protein expression of VSP in the tails of mature sperm (Fig. 1 *A* and *B*, see *SI Appendix*, Fig. S1*B* for VSP$^{-/-}$ mice). Therefore, we

Significance

Voltage-sensing phosphatase (VSP) is a unique protein that consists of both the voltage-sensor domain and phosphoinositide phosphatase domain. In contrast with intensive studies on its molecular mechanisms, its physiological role has not been clear. Here, we report that VSP plays critical roles in mouse sperm motility. We found that VSP generates a polarized distribution of PtdIns(4,5)P_2 in the sperm flagellum, which is critical for regulation of ion channel activity and calcium influx in sperm function. This provides a mode of regulation of ion channel activity by biased distribution of PtdIns(4,5)P_2.

Author contributions: T.K., M.I., and Y.O. designed research; T.K., H.M., H.N., S.S., S.M., J.S., M.W., K.S., and T.F. performed research; H.N., M.W., K.S., and T.S. contributed new reagents/analytic tools; T.K., H.M., H.N., S.M., T.F., T.S., and M.I. analyzed data; and T.K. and Y.O. wrote the paper.

The authors declare no competing interest.

This article is a PNAS Direct Submission.

[1]Present address: Department of Physiology, Faculty of Medicine, Osaka Medical College, Takatsuki 569-8686, Japan.

[2]Present address: Research Institute for Diseases of Old Age, Graduate School of Medicine, Juntendo University, Tokyo 113-8421, Japan.

[3]To whom correspondence may be addressed. Email: yokamura@phys2.med.osaka-u.ac.jp.

This article contains supporting information online at https://www.pnas.org/lookup/suppl/doi:10.1073/pnas.1916867116/-/DCSupplemental.

First published November 27, 2019.

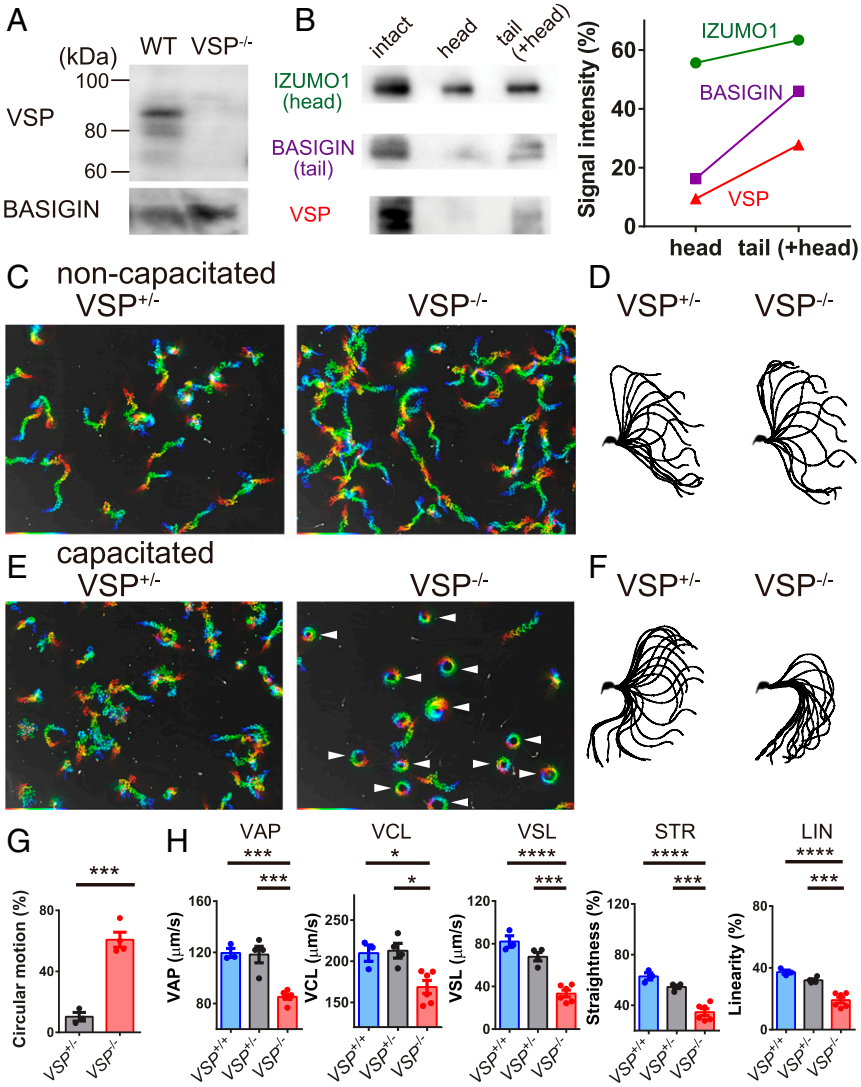

Fig. 1. VSP is expressed in tails of sperm and regulates the motility. (*A*) Western blotting shows VSP signal is specifically observed in sperm of WT. See *Materials and Methods* for details of the VSP-deficient mice. (*B*) To examine the subcellular localization of VSP in sperm, we separated heads from tails. The signal intensity of head and tail (+head) samples, normalized to an intact sperm sample, is shown on the *Right*. The localization of the VSP signal corresponds well to the BASIGIN (tail) signal. (*C*) Trajectories of noncapacitated sperm isolated from $VSP^{+/-}$ and $VSP^{-/-}$ mice. The sperm were incubated for only 5 min in TYH. Each rainbow line indicates each trajectory. (*D*) Flagellar bending patterns of noncapacitated sperm from $VSP^{+/-}$ and $VSP^{-/-}$ mice. (*E*) Trajectories of sperm isolated from $VSP^{+/-}$ and $VSP^{-/-}$ mice after 2 h in TYH (during capacitation). (*F*) Flagellar bending patterns of sperm from $VSP^{+/-}$ and $VSP^{-/-}$ mice during capacitation. (*G*) The proportion of sperm showing circular motion. (*H*) Quantitation of sperm motility parameters at 2 h after TYH incubation. VAP, average path velocity; VCL, curvilinear velocity; VSL, straight-line velocity; STR, straightness; and LIN, linearity. *, ***, and **** indicate significant difference: $P < 0.05$, $P < 0.001$, and $P < 0.0001$, respectively.

examined the physiological importance of VSP in sperm. Although no obvious difference in litter size was seen in breeding pairs with $VSP^{-/-}$ vs. wild-type (WT) males (*SI Appendix*, Fig. S1*C*), we found that VSP-deficient sperm showed a greatly reduced ability to fertilize eggs in vitro (*SI Appendix*, Fig. S1*D*). VSP-deficient sperm showed normal morphology (*SI Appendix*, Fig. S2 *A* and *B*), and both the acrosomal reaction and tyrosine phosphorylation occurred normally during capacitation (*SI Appendix*, Fig. S2 *C* and *D*). However, sperm motility during capacitation of $VSP^{-/-}$ mice was much different from $VSP^{+/-}$ mice (Fig. 1 *C*–*H*).

At only 5 min after incubation in Toyoda, Yokoyama, Hoshi (TYH) medium, which is well established, capacitation-inducing medium (but 5 min is not enough to induce capacitation) (11), the noncapacitated sperm from both $VSP^{+/-}$ and $VSP^{-/-}$ mice showed relatively straight trajectories, with no difference in motility parameters (Fig. 1 *C* and *D* and *SI Appendix*, Fig. S3). We then analyzed the sperm motility at 2 h TYH incubation, which triggers capacitation. While sperm of $VSP^{+/-}$ mice showed a typical asymmetric motility pattern called hyperactivation (Fig. 1*E* and Movie S1), a substantial portion of VSP-deficient sperm showed just circular motion (Fig. 1 *E*–*G* and Movie S2). This appeared to be due to the loss of flexibility in the midpiece and proximal principal piece (Fig. 1*F*). All motility parameters were also significantly decreased in VSP-deficient sperm (Fig. 1*H*).

VSP Regulates PIPs Level in Mouse Sperm. VSP dephosphorylates several classes of PIPs, such as PtdIns(3,4,5)P_3, PtdIns(4,5)P_2, and PtdIns(3,4)P_2 (3, 12, 13). Therefore, we examined the PIPs profiles in sperm of each genotype before and during capacitation by the liquid chromatography tandem mass spectrometry (LC-MS/MS) method (Fig. 2). We found that VSP-deficient

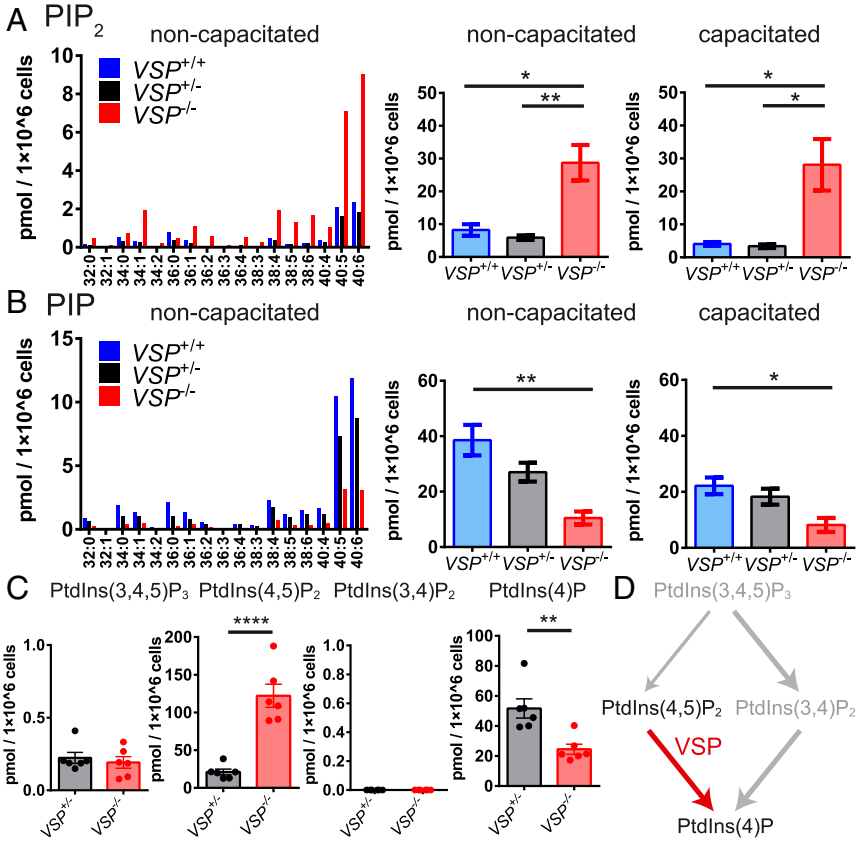

Fig. 2. PIPs profiles for sperm of each genotype. (*A* and *B*) Amount of PIP_2 (*A*) or PIP (*B*) in sperm of each genotype. *Left* shows the profile of PIP_2 (*A*) or PIP (*B*) due to sn-1 and sn-2 acyl chains before capacitation (5 min TYH incubation). Sperm phospholipids showed abundant 40:5 and 40:6 unlike other tissues which primarily contain 38:4. This is probably because sperm contain enriched DPA (22:5) and DHA (22:6) (38). The data are the averaged value from 3 animals for each genotype. *Right* shows the total amount of PIP_2 or PIP before (5 min TYH incubation) and during capacitation (2 h TYH incubation). $n = 3$ for each genotype. (*C*) Total amount of $PtdIns(3,4,5)P_3$, $PtdIns(4,5)P_2$, $PtdIns(3,4)P_2$, and PtdIns(4)P in sperm of $VSP^{+/-}$ and $VSP^{+/+}$ mice. Values under the detection level were set to 0. (*D*) Schematic diagram of VSP activity in mouse sperm. The previous in vitro experiments suggest that VSP targets $PtdIns(3,4,5)P_3$, $PtdIns(4,5)P_2$, and $PtdIns(3,4)P_2$ (gray and red arrows). However, in mouse sperm, VSP only converts $PtdIns(4,5)P_2$ into PtdIns(4)P (red arrow). *, **, and **** indicate a significant difference: $P < 0.05$, $P < 0.01$, and $P < 0.0001$, respectively.

sperm showed a significantly higher total PIP_2 level, and this level did not change during capacitation (Fig. 2 *A*, *Right*). Conversely, the total PIP level in VSP-deficient sperm was significantly reduced (Fig. 2 *B*, *Right*). An increased PIP_2 level and a reduced PIP level in VSP-deficient sperm was observed for almost all types of acyl chains (Fig. 2 *A* and *B*, *Left*).

To further investigate the phosphorylation status of PIPs, we used another MS-based method that differentiates each regioisomer of PIPs. Consistent with Fig. 2 *A* and *B*, VSP-deficient sperm exhibited a decrease in PtdIns(4)P, with a concomitant accumulation of $PtdIns(4,5)P_2$ (Fig. 2*C* and *SI Appendix*, Fig. S4). On the other hand, the level of $PtdIns(3,4,5)P_3$ was comparable between sperm of $VSP^{+/-}$ and $VSP^{-/-}$ mice, and $PtdIns(3,4)P_2$ was barely detected (Fig. 2*C*). These results clearly indicate that VSP functions in a sperm to convert $PtdIns(4,5)P_2$ to PtdIns(4)P (Fig. 2*D*).

Ca^{2+} Influx Is Responsible for the Motility Defect in VSP-Deficient Sperm. One of the critical events occurring in sperm capacitation is Ca^{2+} influx mediated by CatSper, a sperm-specific Ca^{2+} channel located on the flagellum (5, 6). We compared the TYH-induced Ca^{2+} signal in the head and tail of sperm from both genotypes (Fig. 3 *A* and *B*). We found that tails, but not heads, of VSP-deficient sperm showed an enhanced Ca^{2+} response compared with sperm of $VSP^{+/-}$ mice (Fig. 3*B*). Furthermore, when we incubated VSP-deficient sperm in low Ca^{2+} TYH for 2 h, the abnormal motility was significantly reduced (Fig. 3 *C–E* and *SI Appendix*, Fig. S5), indicating that enhanced Ca^{2+} influx is involved in the motility defect in VSP-deficient sperm.

Mechanism Underlying Enhanced Ca^{2+} Influx in VSP-Deficient Sperm Tails. There are two primary Ca^{2+} permeable proteins on sperm flagellum: a sperm-specific Ca^{2+} channel, CatSper (5) and a Ca^{2+} pump, PMCA4 (10). We performed perforated patch-clamp experiments from sperm to record CatSper monovalent current. There was no prominent difference in current amplitudes between $VSP^{+/-}$ and $VSP^{-/-}$ mice (*SI Appendix*, Fig. S6*A*). Furthermore, when we compared the Ca^{2+} response in the tails of sperm from $VSP^{+/-}$ and $VSP^{-/-}$ mice in the presence of a PMCA4 inhibitor, aurintricarboxylic acid (ATA), the increased Ca^{2+} response in the tail of VSP-deficient sperm was still observed (*SI Appendix*, Fig. S6*B*). Therefore, these membrane proteins are unlikely to contribute to the abnormal Ca^{2+} response in VSP-deficient sperm.

Alternatively, we focused on Slo3, a sperm-specific K^+ channel (8), which controls Ca^{2+} influx through CatSper (14) and is activated by $PtdIns(4,5)P_2$ (15) (see also *SI Appendix*, Fig. S7). To examine this, we performed perforated patch-clamp recording, which maintains the intracellular environment. With this condition, sperm showed a relatively depolarized membrane potential (-12 ± 1.6 mV; 19 cells from $VSP^{+/-}$ mice). We pharmacologically isolated Slo3 current as follows: Zeng et al. (8) already

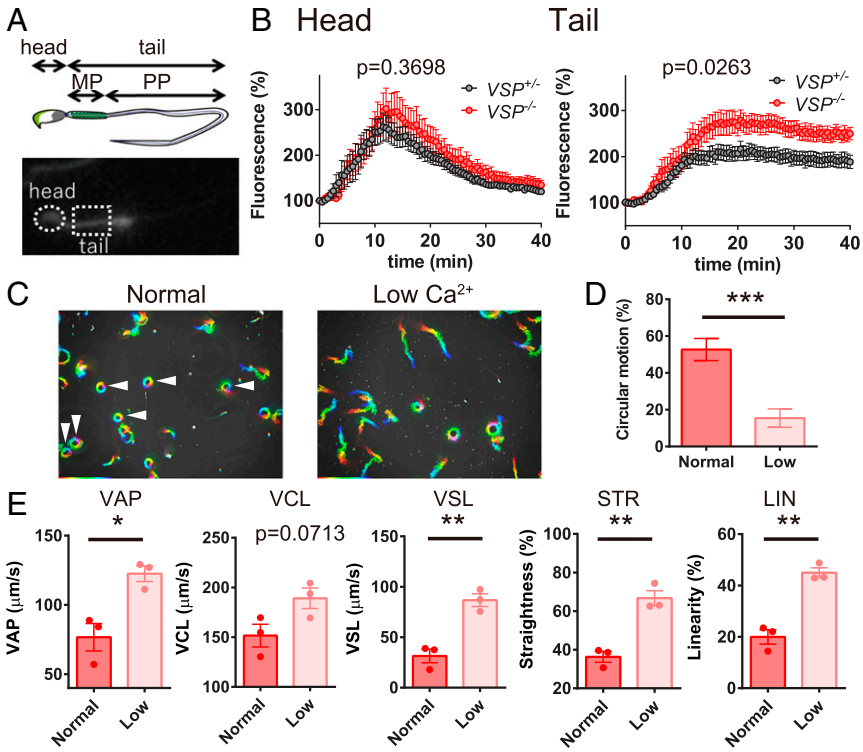

Fig. 3. Enhanced Ca^{2+} response in VSP-deficient sperm regulates sperm motility. (*A*) Representative image of Fluo3 fluorescence in a spermatozoa. (*B*) Time course of the Ca^{2+} response in the head and tail (2-way ANOVA). The significant difference was observed only in tail. (*C–E*) Effect of reducing extracellular Ca^{2+} on motility of VSP-deficient sperm. In the low Ca^{2+} treatment group, the extracellular Ca^{2+} was reduced from 1.7 mM to 0.17 mM. (*C*) Trajectories of sperm isolated from $VSP^{-/-}$ mice after 2 h incubation in normal or low Ca^{2+} TYH. Each rainbow line indicates the trajectory of a sperm. Arrowheads indicate sperm showing circular motion. (*D*) Statistic data showing the proportion of sperm which exhibited circular motion (unpaired *t* test). (*E*) Quantitation of sperm motility parameters after 2 h incubation in normal or low Ca^{2+} TYH. There was a significant difference between the 2 groups. See also *SI Appendix*, Fig. S5 that shows the sperm motility parameters at 5 min incubation. As shown in *SI Appendix*, Fig. S3 and Fig. 1*H*, in normal Ca^{2+} TYH, all parameters for VSP-deficient sperm were drastically reduced (unpaired *t* test). VAP, average path velocity; VCL, curvilinear velocity; VSL, straight-line velocity; STR, straightness; and LIN, linearity. *, **, and *** indicate a significant difference: $P < 0.05$, $P < 0.01$, and $P < 0.001$, respectively.

reported that clofilium, one of the potassium channel blockers, irreversibly suppresses the Slo3 component, while it also reversibly suppresses the CatSper component in native sperm. Therefore, we were able to isolate Slo3 current as the component that was irreversibly inhibited by clofilium (Fig. 4 *C* and *D*). While the isolated Slo3 current was tiny, possibly due to acidic intracellular pH in sperm (16) which suppresses Slo3 (8, 17), sperm from $VSP^{-/-}$ mice showed significantly higher currents than $VSP^{+/-}$ mice (Fig. 4 *A–D*).

We also performed conventional whole-cell patch clamp, and the Slo3 current was enhanced by setting intracellular pH to 8.0 (see also *SI Appendix*, Fig. S8). We still observed enhanced Slo3 current in VSP-deficient sperm in this condition (Fig. 4 *E* and *F*). On the other hand, when we included $PtdIns(4,5)P_2$ antibody in the pipette to cancel the potential effect of $PtdIns(4,5)P_2$, the difference was no longer observed (Fig. 4 *E* and *F*). We also confirmed that protein expression level of Slo3 was not different between sperm of $VSP^{+/-}$ and $VSP^{-/-}$ mice (*SI Appendix*, Fig. S9 *A* and *B*). These results indicate that increased Slo3 activity in VSP-deficient sperm was not due to a difference in protein expression level but rather due to channel activity.

Furthermore, we treated sperm with 1 μM of the K^+ ionophore valinomycin, to cancel the changed Slo3 activity, and observed the Ca^{2+} response in capacitation. Sperm of $VSP^{+/-}$ and $VSP^{-/-}$ mice showed similar Ca^{2+} responses at the sperm tail (*SI Appendix*, Fig. S9*C*), suggesting that abnormal Ca^{2+} response in tails of VSP-deficient sperm is mediated by the altered Slo3 activity.

VSP Is Required for a Heterogeneous Distribution of $PtdIns(4,5)P_2$ along the Longitudinal Axis of the Sperm Tail. Our data suggest that Slo3 activity is affected by PIP profile in VSP-deficient sperm. Among PIPs, $PtdIns(4,5)P_2$ is an especially potent regulator of ion channels, as represented by M-current, which was first identified in frog sympathetic neurons and now widely found in various neurons (18). The activity of the KCNQ2/3 K^+ channel is regulated by the change in $PtdIns(4,5)P_2$ level similarly to Slo3 (19). However, the binding affinity of KCNQ2/3 to $PtdIns(4,5)P_2$ is reported to be much lower than Slo3 (15, 20) (see also Fig. 5*A* and *SI Appendix*, Fig. S10). Low $PtdIns(4,5)P_2$ affinity of KCNQ2/3 (green curve in Fig. 5*A*) makes it possible for the channel to be easily regulated by the change in $PtdIns(4,5)P_2$ at the plasma membrane of a regular somatic cell (gray box in Fig. 5*A*). Therefore, in order to properly regulate Slo3, the $PtdIns(4,5)P_2$ level must be adjusted in the range of the high $PtdIns(4,5)P_2$ affinity of Slo3 (orange box in Fig. 5*A*), at least in the principal piece where Slo3 is selectively present (17).

This hypothesis motivated us to visualize the $PtdIns(4,5)P_2$ distribution in sperm tails. We performed freeze-fracture electron microscopy (EM) to label $PtdIns(4,5)P_2$. This method was verified to capture the lipid distribution with minimal artifact (Fig. 5*B*) (21, 22). Notably, there is a substantial proportion of $PtdIns(4,5)P_2$-poor regions in sperm tails, which have not previously been reported for any cell types to our knowledge (46% for areas of ~100 labels/μm^2; Fig. 5 *C* and *D*). Furthermore, we found that there is a significant positive correlation between tail width and labeling density (Fig. 5 *E*, *Left*; Pearson's correlation coefficient $r = 0.41$ with $P = 0.0002$, $n = 81$), indicating a biased

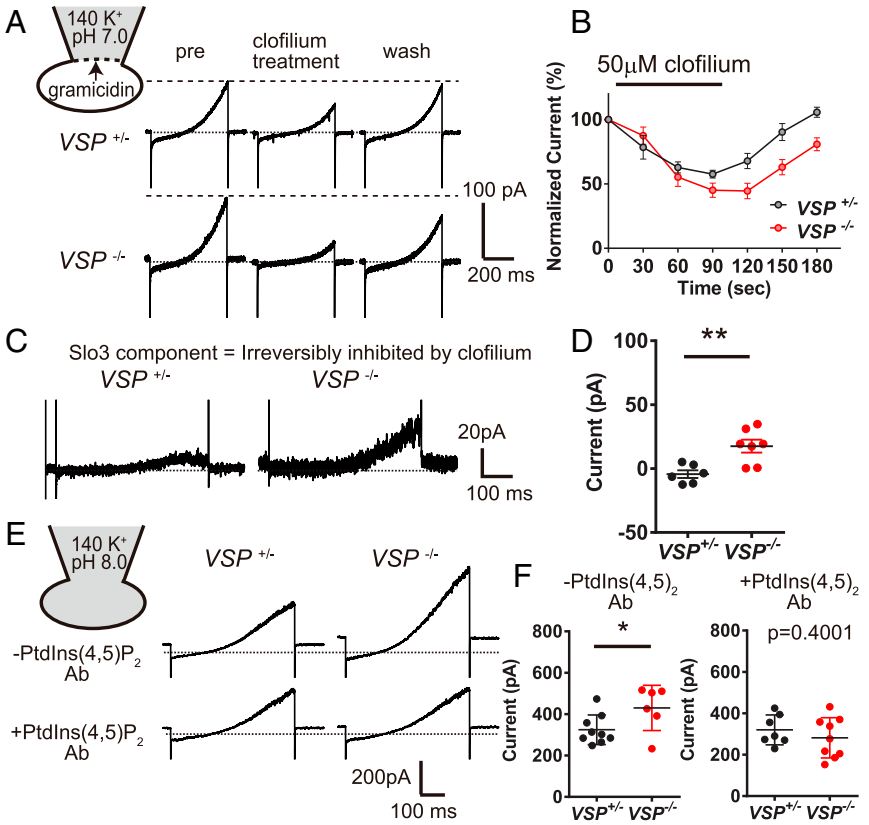

Fig. 4. Slo3 current is enhanced in VSP-deficient sperm. (*A*) Representative current traces before (pre), during (treatment), and after (wash) 50 μM clofilium treatment in perforated patch clamp. A ramp pulse from −100 mV to +100 mV was applied. (*B*) Time course of the change in current amplitude at +100 mV in response to 50 μM clofilium. There was significant difference between genotypes (2-way ANOVA, $P < 0.05$). (*C*) The Slo3 current (irreversible component) was obtained by subtracting the traces at 180 s from the traces at 0 s in *B*. (*D*) Statistical data showing Slo3 current amplitude at +100 mV. (*E*) Representative traces from sperm of $VSP^{+/-}$ and $VSP^{-/-}$ mice with or without PtdIns(4,5)P_2 antibody in whole-cell patch clamp. A ramp pulse from −100 mV to +100 mV was applied. (*F*) Statistical data showing current amplitude at +100 mV. * and ** indicate a significant difference: $P < 0.05$ and $P < 0.01$, respectively.

PtdIns(4,5)P_2 distribution along the longitudinal axis. In contrast, VSP-deficient sperm showed a different pattern of plot distribution ($r = 0.19$ with $P = 0.23$, $n = 40$) (Fig. 5 *E*, *Right*).

Next, we defined principal piece and midpiece based on the tail widths (*SI Appendix*, Fig. S11). While we observed a significant difference in total labeling between the genotypes (Fig. 5*F*), labeling in midpiece showed no significant difference (Fig. 5*G*). On the other hand, the principal piece showed a remarkable difference; The median (interquartile range [IQR]) value was 31 (5.7) labels/μm^2 in $VSP^{+/-}$ mice and 253 (9.8) labels/μm^2 in $VSP^{-/-}$ mice, respectively (Fig. 5*H*). Taken together, VSP appears to generate the biased distribution of PtdIns(4,5)P_2 along the flagellum.

Discussion

We found that VSP in mouse sperm converts PtdIns(4,5)P_2 into PtdIns(4)P and regulates sperm motility during capacitation. Most interestingly, we found that sperm show a heterogeneous PtdIns(4,5)P_2 distribution in their flagellum, with minimal density in the principal piece, and this heterogeneous distribution is not present in sperm lacking VSP. The extraordinarily low level of PtdIns(4,5)P_2 in the principal piece is consistent with the high PtdIns(4,5)P_2 affinity of Slo3, which is regulated by VSP.

VSP Controls Sperm Motility during Capacitation. We found that the function of VSP is related to the capacitation. Interestingly, we found that most of VSP-deficient sperm showed circular motion during capacitation. It is noteworthy that the direction of sperm rotation is uniform and this is due to curvature caused by the lack of flexibility in VSP-deficient sperm (Fig. 1*F*). Many reports suggest that cytosolic Ca^{2+} plays a crucial role in determining the patterning of the flagellar beating (23). Two different genetic experiments indicated that the Ca^{2+} signaling proteins, calcineurin and CatSperζ, affect the flexibility of the midpiece in a similar manner (24, 25). These observations are consistent with our present idea that abnormally elevated Ca^{2+} signaling in VSP-deficient sperm results in a rigid flagellum.

It was surprising that $VSP^{-/-}$ males have no defect in fertility in vivo (*SI Appendix*, Fig. S1*C*) despite the great reduction in in vitro fertilization assay (*SI Appendix*, Fig. S1*D*). Possibly, there may be some compensatory mechanism for reducing the PtdIns(4,5)P_2 level of sperm in vivo, such as stimulation of GPCR or tyrosine kinase receptors. Alternatively, it is also possible that suppression of Ca^{2+} influx by some seminal factor is involved in this difference (26).

VSP in Mouse Sperm Is Activated at the Native Resting Membrane Potential. The present study indicates that VSP exhibits phosphatase activity before capacitation. Our measurements with a perforated patch-clamp method showed that mouse sperm have a relatively depolarized membrane potential (about −12 mV). This result is supported by previous studies using voltage-sensitive dyes showing that noncapacitated mature sperm have a relatively depolarized membrane potential (27).

So far it has not been possible to measure the voltage dependence of mouse VSP, due to its poor targeting to plasma membrane in heterologous expression systems (28). However, there are many reports about voltage dependence of VSP in

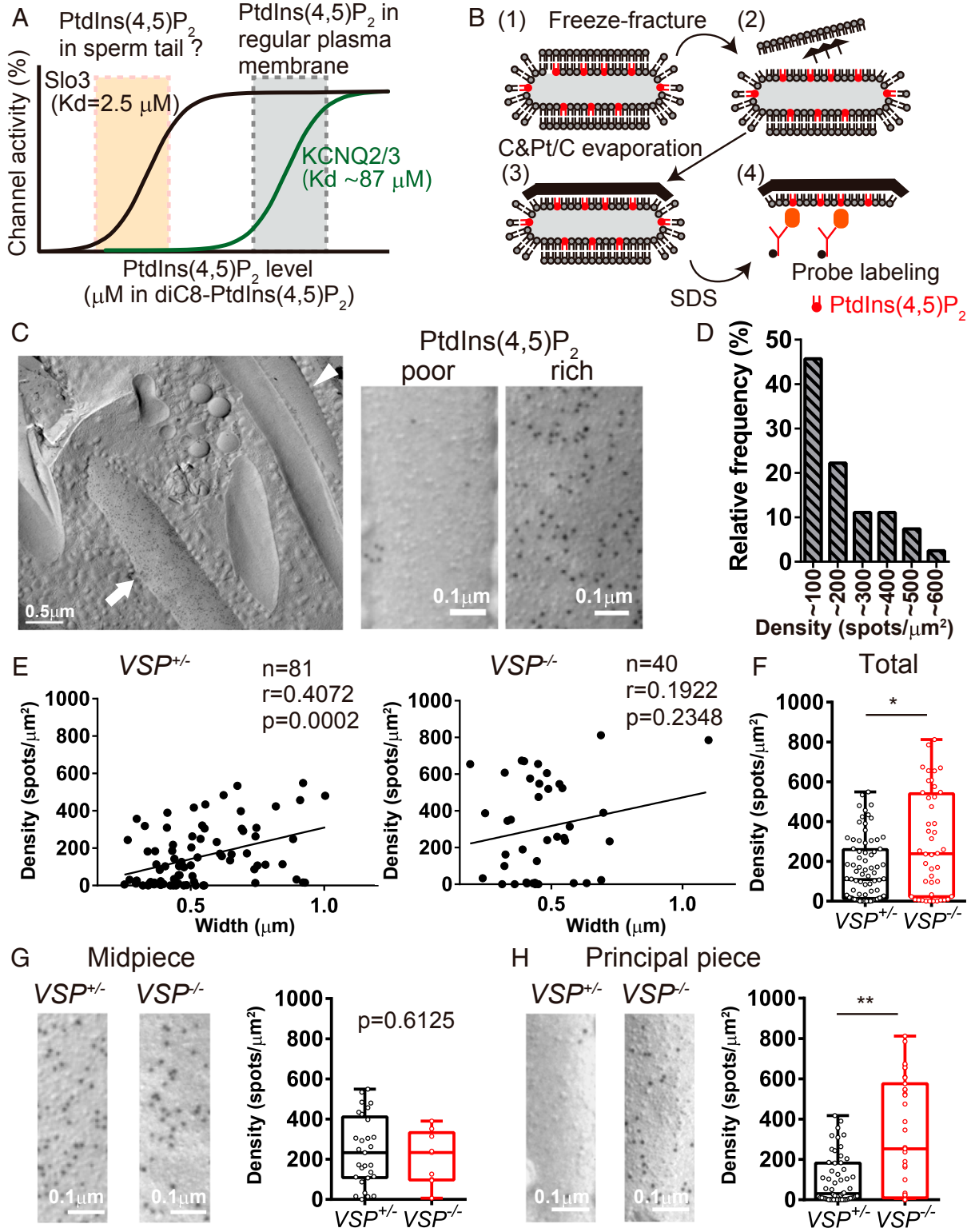

Fig. 5. Localization of PtdIns(4,5)P_2 in freeze-fracture EM of mouse sperm. (*A*) Schematic image showing the relationship between ion channel activity and its PtdIns(4,5)P_2 affinity. (*B*) Outline of the method. For detail, see *Materials and Methods*. (*C*, *Left*) Representative image of PtdIns(4,5)P_2 labeling in sperm from a VSP$^{+/-}$ mouse. Whereas the left tail shows abundant PtdIns(4,5)P_2 labeling (arrow), the right tail shows poor labeling (arrowhead). (*C*, *Right*) Magnified images of the regions indicated by the arrowhead (PIP_2 poor) or arrow (PIP_2 rich). (*D*) Relative frequency of labeling densities (labels/μm^2) in tails of VSP$^{+/-}$ mice. (*E*) Scatterplots showing the relationship between the tail width and the labeling density. (*F*) Statistical data for total population (Mann–Whitney *U* test). (*G*) Data analysis for midpiece. (*Left*) Representative images. (*Right*) Statistical data (Mann–Whitney *U* test). (*H*) Data analysis for principal piece. (*Left*) Representative images. (*Right*) Statistical data (Mann–Whitney *U* test). * and ** indicate a significant difference: $P < 0.05$ and $P < 0.01$, respectively.

other animal species (3, 4, 29). While the voltage dependence of VSP varies slightly among animal species, the threshold for activation is usually close to 0 mV, and some activation occurs even at negative voltages. Furthermore, the Q-V curve of VSP shows a leftward shift with prolonged depolarization, called the "relaxed state" (30), suggesting that constant depolarization may allow the activation of VSP at more negative membrane potentials than reported. Therefore, VSP appears to be weakly but constitutively activated at the resting membrane potential of mouse sperm.

VSP Indirectly Regulates Calcium Signaling. In the present study, we found that VSP indirectly contributes to Ca^{2+} influx by regulating Slo3 activity. A previous report revealed that Slo3 controls Ca^{2+} entry in capacitated sperm through CatSper (14). While the detailed mechanism is not fully understood, Chavez et al. (14) propose that Slo3 promotes a rise in intracellular pH in a voltage-dependent manner through sNHE and/or a bicarbonate transporter-mediated mechanism, promoting Ca^{2+} influx mediated by CatSper. Alternatively, it is also possible that Slo3 simply amplifies the driving force for CatSper-mediated Ca^{2+} influx (31). Activation of Slo3 would induce further hyperpolarization, promoting Ca^{2+} influx by increasing the driving force.

These models also account for why abnormal motility of VSP-deficient sperm only appears during capacitation, despite the fact that VSP is already activated before capacitation. It is already known that Slo3 and CatSper are strongly activated upon capacitation (6, 7). Therefore, the regulation of Slo3 activity by VSP should influence the sperm function more in capacitation processes, especially Ca^{2+} influx mediated by CatSper.

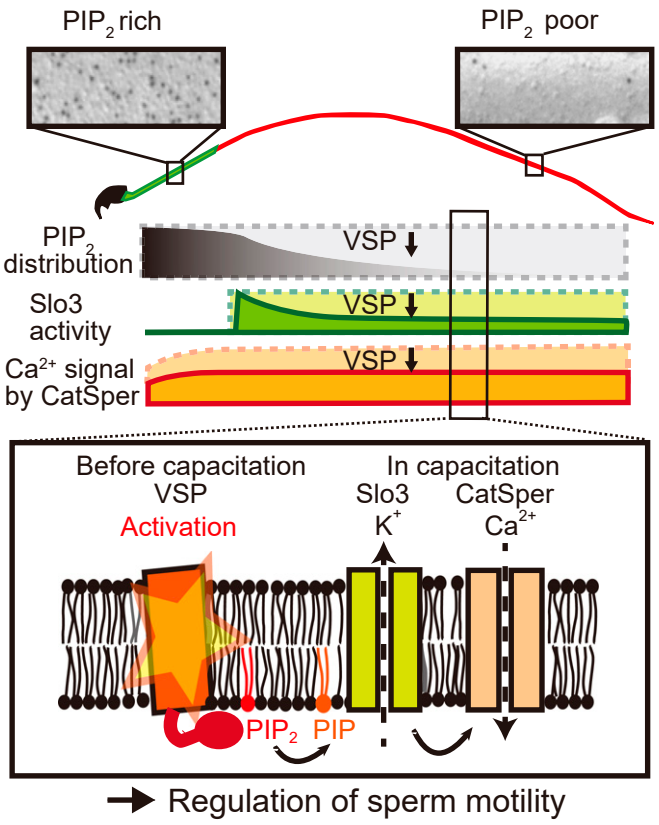

Fig. 6. Schematic illustration showing the present model. VSP generates biased distribution of PtdIns(4,5)P_2 in sperm flagellum. This distribution is important for regulation of Slo3 activity as well as Ca^{2+} influx during capacitation.

Role of the Spatial Distribution of PtdIns(4,5)P_2 in the Sperm Plasma Membrane. Our electrophysiological experiments indicated that the activity of Slo3 is increased in VSP-deficient spermatozoa. The previous studies suggested that the concentration of PtdIns(4,5)P_2 in a normal resting cell is close to the K_d value of the K^+ channel, KCNQ2/3, which is responsible for M-current and sensitive to PtdIns(4,5)P_2; the value is equivalent to 40 to 87 μM diC$_8$-PtdIns(4,5)P_2, water soluble PI(4,5)P_2 (20, 32, 33). Thus, low PtdIns(4,5)P_2-affinity KCNQ2/3 (green curve in Fig. 5*A*) is easily regulated by the change in PtdIns(4,5)P_2 at the plasma membrane (gray box in Fig. 5*A*). On the other hand, Tang et al. (15) reported that EC_{50} of Slo3 is 2.4 ± 0.3 μM diC$_8$-PI(4,5)P_2, indicating the high PtdIns(4,5)P_2 affinity of Slo3. If Slo3 with the high PtdIns(4,5)P_2 affinity (black curve in Fig. 5*A*) is regulated by change of PtdIns(4,5)P_2 concentration at the plasma membrane, the level of PtdIns(4,5)P_2 must be much lower than the regular level (orange box in Fig. 5*A*).

Interestingly, the present study revealed that the principal piece, on which Slo3 is selectively located (17), showed only 31 labels/μm^2 of PtdIns(4,5)P_2 in median value in VSP$^{+/-}$ mouse (Fig. 5*H*). When PtdIns(4,5)P_2 in cultured fibroblasts was labeled using the same protocol, the average labeling density was 422 labels/μm^2 (21), which is more than 10 times in the median value in the normal principal piece. This difference makes sense considering that the K_d value of Slo3 is more than 10 times lower than the concentration of PtdIns(4,5)P_2 in plasma membrane of a regular somatic cell (Fig. 5*A*). We also found that CatSper and PMCA4 activity do not appear to be regulated by such a low concentration of PtdIns(4,5)P_2 (*SI Appendix*, Fig. S6). Thus, the extremely low PtdIns(4,5)P_2 level in the principal piece appears to be specifically adapted for the high-affinity Slo3 channel. In contrast, neurons contain diverse PtdIns(4,5)P_2-sensitive ion channels (K^+ channels, Ca^{2+} channels and others), for example, the low-affinity KCNQ2/3 (2, 3), and also utilize Gq-coupled GPCR signaling, which requires PtdIns(4,5)P_2. Therefore, neurons may require relatively higher PtdIns(4,5)P_2 levels to control their ion channels.

In this study, we report that VSP functions in the regulation of sperm capacitation (Fig. 6). This is an identified function of VSP in a biological system. Because VSP is also expressed in other tissues, such as ovary, brain, and epithelium (3), analysis of VSP function in these tissues would further expand knowledge about the significance of membrane voltage signals. This report proposes that a heterogeneous PtdIns(4,5)P_2 distribution in cells regulates ion channel activity as well as cell function. It will be important to explore in the future whether ion channels with high PtdIns(4,5)P_2 sensitivity in other cell types than sperm can also be regulated by a heterologous distribution of PtdIns(4,5)P_2.

Materials and Methods

Animals. We generated VSP knockin (KI) mice in which the phosphatase domain was truncated at the active catalytic center [Cx5R(T/S) motif] (3, 4, 29) and Venus was fused at the end (*SI Appendix*, Fig. S1*B*). The targeting vector containing the Venus-encoding gene and floxed neomycin cassette, flanked by the 5′ arm of 6.3 kb upstream and the 3′ arm of 5.3 kb downstream of exon 21, was introduced into RENKA, a C57BL/6N-derived embryonic stem (ES) cell line, by electroporation. After selecting G-418-resistant clones, genome recombination was confirmed by Southern blotting. Suitable cell lines were injected into 8-cell-stage embryos of ICR strain and implanted into the uterus of pseudopregnant mothers. Genotypes were determined by PCR analysis using the following primers: WT, forward, 5′-ACATTGGCTATGTCACTAGG-3′; reverse, 5′-TTAACCGCCTGTGTTCGCAC -3′ and KI, forward, 5′-ACATTGGCTATGTCACTAGG-3′; reverse, 5′-ATGGTGCGCTCCTGGACGTAGCC-3′. By Western blotting, we found that sperm of the VSP knockin mice unexpectedly lacked the whole gene product of VSP at the protein level (Fig. 1*A*), suggesting that the product is degraded shortly after translation. All animal procedures were approved by the animal care and use committees of Osaka University and Niigata University.

Drugs and Antibodies. Gramicidin (Merck, Kenilworth, NJ), clofilium tosylate (Merck), goat polyclonal anti-BASIGIN (sc-9757, Santa Cruz Biotechnology, Santa Cruz, CA), anti-PtdIns(4,5)P_2 (915-046, Assay Designs, Ann Arbor, MI), rabbit anti-GST antibody (Bethyl), HRP-linked anti-rabbit or mouse secondary antibody (NA9340V and NA9310V; GE Healthcare, Pittsburgh, PA), and HRP-linked anti-rat or goat secondary antibody (sc-2006 and sc-2020; Santa Cruz Biotechnology) were commercially obtained. A rabbit polyclonal antibody for VSP was raised against the N-terminal residues 140 through 172 of mouse VSP (National Center for Biotechnology Information Reference Sequence: NP_954866). The rat monoclonal anti-IZUMO1 antibody was generated previously (34).

Western Blotting. Sperm from cauda epididymis were rotated at 4 °C for 1 h in a lysis solution containing: 10 mM Tris·HCl (pH 7.5), 50 mM KCl, 1% Triton X-100, and cOmplete Protease Inhibitor Mixture (Roche). After SDS/PAGE for the supernatant, the proteins were transferred to a PVDF membrane. After blocking with 0.5% skim milk or 2% BSA, the blots were incubated with primary antibody: anti-VSP (1:500), anti-IZUMO1 (1:1,000), or anti-BASIGIN (1:500) in PBST or Can get signal 1 (Toyobo, Osaka, Japan). The membranes were washed and incubated with HRP-linked anti-rabbit, rat, or goat antibody (1:1,000) in PBST or Can get signal 2 (TOYOBO). The signals were detected with ECL Prime Western Blotting Detection Reagent (GE Healthcare). Images were acquired using a CS analyzer system (ver. 3) (ATTO, Tokyo, Japan). We sometimes performed antibody stripping using 200 mM glycine (pH 2.8) for 10 min at 60 °C for the other antibody experiments.

For head and tail separation, we modified previous protocols (35). Briefly, sperm isolated from cauda epididymis were divided into 2 groups: no-separation and separation groups. Both were centrifuged at 9,000 × *g* for 5 min at 4 °C and the pellet was snap frozen in liquid nitrogen and diluted with 600 μL of PBS. For the separation group, the sperm suspension was passed 50 times through a 27-gauge needle on ice and centrifuged at 300 × *g* for 5 min at 4 °C to precipitate the sperm heads. Sperm tails were recovered from the supernatant by centrifugation at 9,000 × *g* for 5 min at 4 °C.

Sperm Motility Analysis. Sperm velocity was analyzed as described previously (25). Briefly, spermatozoa isolated from cauda epididymis were suspended in TYH medium, a well-established, capacitation inducing medium (11). TYH contains: 120 mM NaCl, 4.8 mM KCl, 1.2 mM KH_2PO_4, 5.6 mM glucose, 1.0 mM sodium pyruvate, 1.7 mM $CaCl_2$, 1.2 mM $MgSO_4$, 25 mM $NaHCO_3$, 4.0 g/L ALBMAX I (Thermo Fisher Scientific), penicillin (50 units/mL)–streptomycin (50 μg/mL) and 0.6% Phenol red. Average path velocity (VAP), curvilinear velocity (VCL), straight-line velocity (VSL), straightness (STR), and linearity (LIN) were measured using the CEROS sperm analysis system (Hamilton Thorne Biosciences) at 5 min and 2 h after incubation. Sperm motility was videotaped with an Olympus BX-53 microscope equipped with a high-speed camera (HAS-L1, Ditect, Tokyo, Japan) at 200 frames per second. The trajectory was visualized using ImageJ software (NIH) and plug-in Color Footprint Rainbow developed by Y. Hiratsuka (JAIST, Ishikawa, Japan). Waveforms were analyzed using a sperm motion analyzing software (BohBohsoft, Tokyo, Japan).

Calcium Imaging. Sperm were isolated from cauda epididymis into HEPES saline (HS) medium with the following composition (in mM): 135 NaCl, 5 KCl, 2 $CaCl_2$, 1 $MgCl_2$, 30 Hepes, 10 glucose, 10 lactic acid, and 1 sodium pyruvate (pH 7.4). We loaded sperm with 20 μM Fluo3-AM (Dojindo, Kumamoto, Japan) and 0.05% PluorF-127 in HS medium for 40 min at 37 °C. Sperm were washed with HS and incubated on Cell-Tak (Corning, Bedford, MA)-coated round cover glasses for 10 min. The cover glass was mounted on a perfusion chamber. The fluorescence was detected with a filter set (Excitation 495/10; Dichroic mirror 515; Emission 535/25) and recorded using a IX-81 upright microscope (Olympus, Tokyo, Japan) equipped with a C9100 electron multiplying charge-coupled device (EMCCD) camera (Hamamatsu Photonics, Shizuoka, Japan) and Metamorph imaging software (Molecular Devices). Images were acquired every 30 s. To evoke a Ca^{2+} response in sperm, HS was replaced by phenol red-free TYH. Background was subtracted in all recordings. All cells that were in the field of view throughout the recording and that showed a response (more than 150% of the basal value in fluorescence intensity) were used for data analysis. The acquired data were averaged for each experiment.

Electrophysiology. Patch-clamp recording from spermatozoa was performed as previously described (5). Briefly, sperm were isolated from corpus epididymis in an HS-based solution containing (in mM): 135 NaCl, 5 KCl, 2 $CaCl_2$, 1 $MgSO_4$, 20 Hepes, 5 glucose, 10 lactic acid, and 1 sodium pyruvate (pH 7.4). After 10 min, the supernatant was centrifuged, washed twice, resuspended, and put on untreated glass coverslips. In perforated patch recordings for Slo3 current, the intracellular solution contained (in mM): 120 KCl, 3 $MgCl_2$, 40 Hepes, 0.3 EGTA (pH 7.0), and 0.05 mg/mL gramicidin. The above HS-based solution was used for bath solution. After pore formation by antibiotics, access resistance was 50 to 100 MΩ. In conventional whole-cell recordings, we recorded Slo3 current using high pH intracellular solution consisting of (in mM): 120 KCl, 3 $MgCl_2$, 40 Hepes, and 0.3 EGTA (pH 8.0). The above HS-based solution was used for the bath solution. Pipette resistance was 5 to 10 MΩ. Access resistance in the whole-cell configuration was 15 to 50 MΩ. The recordings were made within 30 s after break-in to avoid potential washout of PIP_2. Recording pipettes were made of borosilicate glass (BF-150-86-10; Sutter Instruments) using a puller (P-97; Sutter Instruments). Recordings were performed using an Axopatch 200B (Molecular Devices), and electrical signals were low-pass filtered at 2 kHz and sampled at 5 kHz using Digidata1550A (Molecular Devices) and pCLAMP10.5 software (Molecular Devices).

Mass Spectrometric Analysis of PIPs. Sperm were isolated from cauda epididymis to TYH and the number of cells was counted. Cells were incubated for 5 min or 2 h and centrifuged at 500 × *g* for 5 min, and pellets were frozen in liquid nitrogen. Acidic phospholipids were extracted by the Bligh–Dyer method as described previously (36). PIPs were measured by modifying a method developed by Clark et al. (37). An UltiMate 3000 LC system (Thermo Fisher Scientific) equipped with an HTC PAL autosampler (CTC Analytics) was used for column chromatography. TSQ-Vantage (Thermo Fisher Scientific) was used for electrospray ionization MS/MS analysis. For isoform identification experiments, sperm from cauda epididymis were isolated in HS. Cells were centrifuged at 500 × *g* for 5 min and pellets were frozen in liquid nitrogen and followed by the Bligh–Dyer extraction. A new LC-MS/MS method was used to differentiate the regioisomers of PIP and PIP_2.

Freeze-Fracture Electron Microscopy. Sperm from cauda epididymis were isolated in HS medium, centrifuged at 9,000 × *g* for 5 min at 4 °C, and pellets were quick frozen by using an HPM 010 high-pressure freezing machine (Leica Microsystems, Wetzlar, Germany). For freeze fracture, we modified previous protocols (21, 22). The frozen specimens were transferred to the cold stage of a Balzers BAF 400 apparatus and fractured at −120 °C to −100 °C under a vacuum of ∼1 × 10^(−6) mbar. Replicas were made by electron-beam evaporation in 3 steps: carbon (C) (2 to 5 nm in thickness) at an angle of 90° to the specimen surface, platinum-carbon (Pt/C) (1 to 2 nm) at an angle of 45°, and C (10 to 20 nm) at an angle of 90°. The thickness of the deposition was adjusted by referring to a crystal thickness monitor. Thawed replicas were treated overnight with 2.5% SDS in PBS at 60 °C and digested with 0.4 mg/mL of DNaseI (Sigma) in 40 mM Tris·HCl (pH 7.9), 100 mM NaCl, 6 mM $MgCl_2$, and 1 mM $CaCl_2$ for 2 d at 37 °C. The replicas were further digested overnight with 50 μg/mL proteinase K (TAKARA, Shiga, Japan) in 20 mM Tris·HCl (pH 8.0), 10 mM EDTA, 10 mM NaCl, and 0.5% SDS at 60 °C, rinsed with PBS containing 0.1% Tween-20 (PBST), and stored in buffered 50% glycerol at −20 °C until use.

Freeze-fracture replicas were washed with PBST, blocked with a mixture of 3% BSA and 2% cold fish skin gelatin in PBS, and incubated with recombinant GST-tagged pleckstrin homology (PH) domain of phospholipase C (PLC)-δ1 (30 ng/mL) in 1% BSA and 1% cold fish skin gelatin in PBS at 4 °C overnight. The samples were subsequently treated with rabbit anti-GST antibody (10 μg/mL; Bethyl) followed by colloidal gold (10 nm)-conjugated protein A (1:60 dilution of the supplied solution; University Medical Center Utrecht), both for 30 min at 37 °C in 1% BSA in PBS. After each incubation, replicas were washed extensively with 0.1% BSA in PBS. After brief rinses with distilled water, replicas were picked up on formvar-coated EM grids and observed with a JEM-1011 electron microscope operated at 100 kV. Digital images were captured by a CCD camera (Gatan Inc.) and subjected to further analysis. Obtained images were semiautomatically analyzed using ImageJ software. Color inverted 8-bit images were subjected to background subtraction. The processed images were binarized and particles were detected using "Analyze Particles."

Data Analysis. Data analysis was performed with Excel 2016 (Microsoft), Clampfit 10.5 (Molecular Device), and Igor Pro-6.37 (WaveMetrics) software. Statistical analysis was performed with Prism 6 (GraphPad Software, San Diego, CA). For 2-group comparison, we conducted an unpaired *t* test or Mann–Whitney *U* test as appropriate. For multiple comparisons, we conducted Tukey's test. Outliers identified by Grubbs' test were excluded from the analysis. We also conducted 2-way repeated-measures ANOVA when we compared time courses. Data are represented as mean ± SEM or median

PHYSIOLOGY

(IQR) as appropriate. *, **, ***, and **** indicate a significant difference: $P < 0.05$, $P < 0.01$, $P < 0.001$, and $P < 0.0001$, respectively.

Data Availability. All data are available in the manuscript and *SI Appendix*.

ACKNOWLEDGMENTS. We thank Ms. Nana Miyawaki, Ms. Yuko Furukawa, Ms. Yuka Miyoshi, Dr. Hiroki Arima, Ms. Fumiko Takenaga, Ms. Eri Hosoyamada, Dr. Yoshifumi Okochi (Osaka University), Dr. Jinglei Cheng (Nagoya University), and Dr. Satoshi Eguchi (Akita University) for their technical support. Thanks are due to Dr. Manabu Yoshida (University Tokyo) and Dr. Kaoru Yoshida (Toin University of Yokohama) for inspiring discussions. This study was supported by Mr. Eiji Oiki and the Center for Medical Research and Education, Graduate School of Medicine, Osaka University. This work was supported by Dr. Kanji Kasahara (Kasahara OB/GYN Clinic). This work was also supported by Grants-in-Aid from Japan Society for the Promotion of Science (JSPS) (12J01957 and 17K15558) to T.K., and Grant-in-Aid for Scientific Research on Innovative Areas (15H05901) and JSPS (21229003, 25253016, and 19H03401) to Y.O.

1. T. Balla, Phosphoinositides: Tiny lipids with giant impact on cell regulation. *Physiol. Rev.* **93**, 1019–1137 (2013).
2. B. C. Suh, B. Hille, PIP_2 is a necessary cofactor for ion channel function: How and why? *Annu. Rev. Biophys.* **37**, 175–195 (2008).
3. Y. Okamura, A. Kawanabe, T. Kawai, Voltage-sensing phosphatases: Biophysics, physiology, and molecular engineering. *Physiol. Rev.* **98**, 2097–2131 (2018).
4. Y. Murata, H. Iwasaki, M. Sasaki, K. Inaba, Y. Okamura, Phosphoinositide phosphatase activity coupled to an intrinsic voltage sensor. *Nature* **435**, 1239–1243 (2005).
5. Y. Kirichok, B. Navarro, D. E. Clapham, Whole-cell patch-clamp measurements of spermatozoa reveal an alkaline-activated Ca^{2+} channel. *Nature* **439**, 737–740 (2006).
6. D. Ren *et al*., A sperm ion channel required for sperm motility and male fertility. *Nature* **413**, 603–609 (2001).
7. C. M. Santi *et al*., The SLO3 sperm-specific potassium channel plays a vital role in male fertility. *FEBS Lett.* **584**, 1041–1046 (2010).
8. X. H. Zeng, C. Yang, S. T. Kim, C. J. Lingle, X. M. Xia, Deletion of the Slo3 gene abolishes alkalization-activated K+ current in mouse spermatozoa. *Proc. Natl. Acad. Sci. U.S.A.* **108**, 5879–5884 (2011).
9. D. Wang, S. M. King, T. A. Quill, L. K. Doolittle, D. L. Garbers, A new sperm-specific Na^+/H^+ exchanger required for sperm motility and fertility. *Nat. Cell Biol.* **5**, 1117–1122 (2003).
10. K. Schuh *et al*., Plasma membrane Ca^{2+} ATPase 4 is required for sperm motility and male fertility. *J. Biol. Chem.* **279**, 28220–28226 (2004).
11. T. Toyoda, M. Yokoyama, T. Hosi, Studies on the fertilization of mouse eggs in vitro. I. In vitro fertilization of eggs by fresh epididymal sperm. *Jpn. J. Anim. Reprod.* **16**, 147–151 (1971).
12. H. Iwasaki *et al*., A voltage-sensing phosphatase, Ci-VSP, which shares sequence identity with PTEN, dephosphorylates phosphatidylinositol 4,5-bisphosphate. *Proc. Natl. Acad. Sci. U.S.A.* **105**, 7970–7975 (2008).
13. T. Kurokawa *et al*., 3′ Phosphatase activity toward phosphatidylinositol 3,4-bisphosphate [$PI(3,4)P_2$] by voltage-sensing phosphatase (VSP). *Proc. Natl. Acad. Sci. U.S.A.* **109**, 10089–10094 (2012).
14. J. C. Chávez *et al*., SLO3 K^+ channels control calcium entry through CATSPER channels in sperm. *J. Biol. Chem.* **289**, 32266–32275 (2014).
15. Q. Y. Tang, Z. Zhang, J. Xia, D. Ren, D. E. Logothetis, Phosphatidylinositol 4,5-bisphosphate activates Slo3 currents and its hydrolysis underlies the epidermal growth factor-induced current inhibition. *J. Biol. Chem.* **285**, 19259–19266 (2010).
16. Y. Zeng, J. A. Oberdorf, H. M. Florman, pH regulation in mouse sperm: Identification of Na^+-, Cl^--, and $HCO3^-$-dependent and arylaminobenzoate-dependent regulatory mechanisms and characterization of their roles in sperm capacitation. *Dev. Biol.* **173**, 510–520 (1996).
17. B. Navarro, Y. Kirichok, D. E. Clapham, KSper, a pH-sensitive K^+ current that controls sperm membrane potential. *Proc. Natl. Acad. Sci. U.S.A.* **104**, 7688–7692 (2007).
18. D. A. Brown, P. R. Adams, Muscarinic suppression of a novel voltage-sensitive K^+ current in a vertebrate neurone. *Nature* **283**, 673–676 (1980).
19. B. C. Suh, B. Hille, Recovery from muscarinic modulation of M current channels requires phosphatidylinositol 4,5-bisphosphate synthesis. *Neuron* **35**, 507–520 (2002).
20. Y. Li, N. Gamper, D. W. Hilgemann, M. S. Shapiro, Regulation of K_v7 (KCNQ) K^+ channel open probability by phosphatidylinositol 4,5-bisphosphate. *J. Neurosci.* **25**, 9825–9835 (2005).
21. A. Fujita, J. Cheng, K. Tauchi-Sato, T. Takenawa, T. Fujimoto, A distinct pool of phosphatidylinositol 4,5-bisphosphate in caveolae revealed by a nanoscale labeling technique. *Proc. Natl. Acad. Sci. U.S.A.* **106**, 9256–9261 (2009).
22. N. Ozato-Sakurai, A. Fujita, T. Fujimoto, The distribution of phosphatidylinositol 4,5-bisphosphate in acinar cells of rat pancreas revealed with the freeze-fracture replica labeling method. *PLoS One* **6**, e23567 (2011).
23. C. B. Lindemann, J. S. Goltz, Calcium regulation of flagellar curvature and swimming pattern in triton X-100–Extracted rat sperm. *Cell Motil. Cytoskeleton* **10**, 420–431 (1988).
24. J. J. Chung *et al*., CatSperζ regulates the structural continuity of sperm Ca^{2+} signaling domains and is required for normal fertility. *eLife* **6**, e23082 (2017).
25. H. Miyata *et al*., Sperm calcineurin inhibition prevents mouse fertility with implications for male contraceptive. *Science* **350**, 442–445 (2015).
26. S. H. Lu *et al*., Capacitation suppression by mouse seminal vesicle autoantigen involves a decrease in plasma membrane Ca^{2+}-ATPase (PMCA)-mediated intracellular calcium. *J. Cell. Biochem.* **111**, 1188–1198 (2010).
27. I. A. Demarco *et al*., Involvement of a Na^+/HCO_3^- cotransporter in mouse sperm capacitation. *J. Biol. Chem.* **278**, 7001–7009 (2003).
28. Y. Wu *et al*., PTEN 2, a Golgi-associated testis-specific homologue of the PTEN tumor suppressor lipid phosphatase. *J. Biol. Chem.* **276**, 21745–21753 (2001).
29. M. I. Hossain *et al*., Enzyme domain affects the movement of the voltage sensor in ascidian and zebrafish voltage-sensing phosphatases. *J. Biol. Chem.* **283**, 18248–18259 (2008).
30. C. A. Villalba-Galea, W. Sandtner, D. M. Starace, F. Bezanilla, S4-based voltage sensors have three major conformations. *Proc. Natl. Acad. Sci. U.S.A.* **105**, 17600–17607 (2008).
31. J. L. De La Vega-Beltran *et al*., Mouse sperm membrane potential hyperpolarization is necessary and sufficient to prepare sperm for the acrosome reaction. *J. Biol. Chem.* **287**, 44384–44393 (2012).
32. M. Kruse, G. R. V. Hammond, B. Hille, Regulation of voltage-gated potassium channels by $PI(4,5)P_2$. *J. Gen. Physiol.* **140**, 189–205 (2012).
33. H. Zhang *et al*., PIP_2 activates KCNQ channels, and its hydrolysis underlies receptor-mediated inhibition of M currents. *Neuron* **37**, 963–975 (2003).
34. M. Ikawa *et al*., Calsperin is a testis-specific chaperone required for sperm fertility. *J. Biol. Chem.* **286**, 5639–5646 (2011).
35. N. Kong *et al*., Natriuretic peptide type C induces sperm attraction for fertilization in mouse. *Sci. Rep.* **7**, 39711 (2017).
36. J. Sasaki *et al*., The $PtdIns(3,4)P_2$ phosphatase INPP4A is a suppressor of excitotoxic neuronal death. *Nature* **465**, 497–501 (2010).
37. J. D. Clark *et al*., A novel arachidonic acid-selective cytosolic PLA_2 contains a Ca^{2+}-dependent translocation domain with homology to PKC and GAP. *Cell* **65**, 1043–1051 (1991).
38. L. A. Johnson, R. J. Gerrits, E. P. Young, The fatty acid composition of porcine spermatozoa phospholipids. *Biol. Reprod.* **1**, 330–334 (1969).